Performance Limits

W. G. Bagnuolo & T. ten Brummelaar
CHARA, Georgia State University, Atlanta, GA 30303

Q.1. INTRODUCTION

The perimeter of the performance 'envelope' of the CHARA Array determines the useful science that can be done with it. The performance of the CHARA Array can be specified in terms of at least four dimensions:

1. The maximum resolution.
2. The magnitude limit.
3. The size and "complexity" of the object.
4. The wavebands in which the Array operates.

The CHARA Array is designed to operate primarily in the regions 0.55–0.9 μm ($\approx V$, R, and I) and 2.1–2.5 μm ($\approx K$). These wavebands were chosen because the classes of scientific programs tended to have a bimodal distribution, requiring either high resolution of relatively simple objects in the visual or lower resolution of larger more complex objects in the K-band IR.

Given these desired wavebands, the ability to image objects is given by the first three performance criteria. (We use the term "image" broadly, including determining the diameters of stars, their limb-darkening, etc. − i.e. the lowest moments of the object that can be determined from visibilities only.) In the rest of this report we will estimate the resolution limits, magnitude limits, and how well various objects can be imaged by the CHARA Array.

Q.2. RESOLUTION LIMITS

Figure Q.1 shows the anticipated limits of the Array in terms of the size and visual magnitudes of representative stellar photospheres. Note that for these performance limits, samples of virtually all spectral types of stars can be resolved, even M dwarfs and O stars. It can be seen from this figure that the CHARA array offers only a slight increase in limiting magnitude over existing speckle techniques, but a gain of at least two orders of magnitude in resolution. The approximate maximum resolution of the Array is given by the first nulls of the visibilities, which are $\theta \approx 1.22\lambda/D$ for resolved stars and $\theta \approx 0.5\lambda/D$ for unresolved binaries. By moving three of the seven telescopes, the Array can be reconfigured for higher or lower angular resolution. The longest baselines in array configurations "A" and "B" are 354 and 199 m respectively, which correspond to the angular resolutions given in Table Q.1.

Q.2.1. Brown Dwarf/Planet Search

In speckle interferometry, a kind of "super-resolution" can be obtained of the motion of a third body about the orbit of a binary star (see Cole et. al. 1992 for an example). In speckle interferometry, the orbit of a binary can be determined to precision of better than 1 mas, or 3% of an Airy disk. A similar advantage with the CHARA Array can be anticipated.
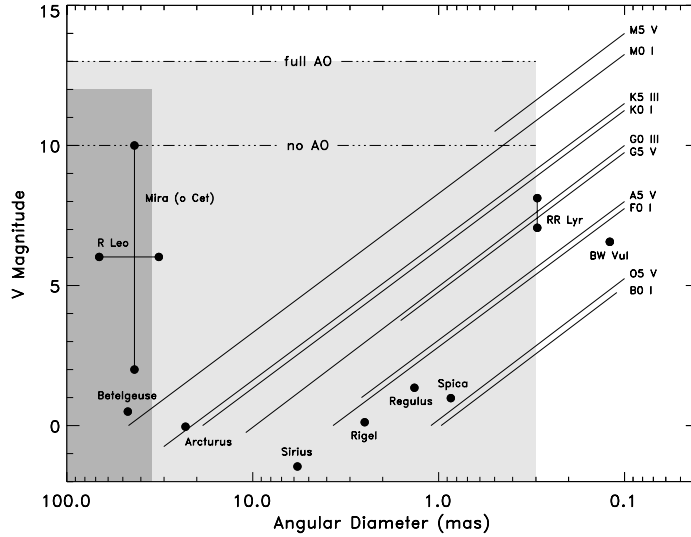
FIGURE Q.1. Magnitudes and sizes of representative stellar types. The darker shading indicates the range accessible to speckle interferometry, while the lighter shading indicates the range (with and without adaptive optics) accessible to the proposed CHARA Array.

TABLE Q.1. Resolution limits for CHARA Array, in milliarcseconds.

Object	Config.	550 nm	900 nm	2200 nm
Binary	A	0.160	0.262	0.641
	B	0.285	0.466	1.140
Res. Star	A	0.391	0.640	1.560
	B	0.696	1.138	2.782

Simulations with the CHARA Array layout have shown that a point on a binary star orbit can be determined to a precision of as small as 10–20 micro-arcsec (μas). This is more than enough to detect Jovian-type planets at 10 pc, which would typically cause a motion of 100 μas.

Q.3.   MAGNITUDE LIMITS

There are three servo systems in the Array:

1. Fringe-tracking (Zernike n=1).

2. Tip-tilt (n=2,3).

3. Higher order Adaptive Optics (AO) (n >3).

These systems, along with the detector system, determine the limiting magnitude (and visibility losses) for the Array. As in a chain, the weakest link determines the magnitude limit for the system as a whole. Typically, as we shall see, the fringe-tracking system has the worst magnitude limit. Therefore, we should obtain the highest possible collecting aperture consistent with maintenance of good fringe visibility in order to get more photons into the fringe-tracking system. However, if an AO system is used, the limiting magnitude decreases with the number of actuators or Zernike modes corrected, and at some point the magnitude limit from the AO system becomes worse than that from the fringe-tracking system. Therefore, it is important to estimate the effect of the degree of AO compensation for the proposed 1 m apertures. Ideally, we would like an AO system with the fewest Zernike modes, and therefore the highest magnitude limit, consistent with high visibility ($V \geq 0.7$). [A description of the AO options is given in Appendix S.]

Q.3.1. Description of Simulations and Results

We obtained the results of realistic simulations of an AO system tailored to the CHARA Array from a group at Science Applications International Corp. (SAIC), headed by Dr. Russ Vernon. Simulations were done to estimate the effect of the degree of AO compensation. The three cases considered were AO systems that correct for various Zernike modes:

1. 3 (tip/tilt)
2. 6 (defocus and astigmatism)
3. 21

The simulations include diffraction effects and four sources of noise:

1. Fitting error — the wavefront cannot be completely matched by the degree of Zernike terms.
2. Servo lag — 40 Hz bandwidth was used, with 5 ms integration times.
3. Processor lag — 3.5 ms was used.
4. Photon noise – for the case with 30 photons/actuator.

Again, an AO system with the fewest Zernike modes consistent with high visibility ($V \geq 0.7$) is desirable. Table Q.2 shows the results of both simulations and analytical calculations from SAIC. Note first that Strehls of ≈ 0.7 are attained only with $\approx (D/r_o)^2$ actuators, i.e. one actuator for every r_o diameter patch on the aperture. For one-fourth as many actuators (every $2 \times r_o$ diameter patch), the Strehl is about 0.4.

In Table Q.2, the servo lag due to a 5 ms sampling rate and 40 Hz bandwidth appears acceptable. The additional loss of Strehl ratio from the processor lag, assumed to be 3.5 ms, is significant. Of this, 2.5 ms of the processor lag comes from the 5 ms sampling rate, and 1.0 ms comes from the actual speed of computation. A good control system should largely eliminate this latter source of error, and for this somewhat pessimistic atmospheric model, a sample time in the range of 3 ms should improve the former source. Finally, we note an additional loss due to photon noise, assumed to arise from 30 photons per AO element. As shown in Appendix S, 50 per element is a safer target to minimize this loss.

We performed additional simulations to examine the relation between Strehl ratio and visibility amplitudes, by combining beams from three 'telescopes' together in a simple non-redundant pattern. Figure Q.2 shows one typical fringe pattern. Note the three fringe

TABLE Q.2.   Strehl ratio results ($\approx$visibilities)

$r_\circ$	Zernike Mode	Fit Error	FE + Servo Lag	FE + SL + Proc. Lag	FE + Sl + Pl + Photon Noise
20 cm	3	0.25	0.24	0.17	0.13
	6	0.40	0.38	0.29	0.23
	10	0.56	0.53	0.40	0.33
	21	0.73	0.68	0.54	0.45
10 cm	3	0.04	0.04	0.02	0.02
	6	0.07	0.065	0.05	0.045
	10	0.18	0.16	0.09	0.08
	21	0.38	0.34	0.18	0.16

patterns in the x-direction, y-direction, and diagonally from upper left to lower right. The fringe spacing (relative tilt of beams from telescopes B and C) was set to produce fringes with spatial frequencies of 10 units differences in x and y. The 61$\times$61 complex numbers defining the apertures were embedded into 128$\times$128 complex arrays.

Figures Q.3 and Q.4 show the average fringe amplitudes (visibilities) for an average of 200 frames for a case with good seeing and high-order AO. The corresponding Strehl ratio, calculated by SAIC, was 0.54, very close to the normalized fringe visibilities for both the 3-beam and 2-beam combination cases (0.55 and 0.54 respectively).

We can check this result by referring to the simple analytical AO model described in Appendix S. The Strehl is given by $S = exp(-\sigma^2)$, where σ^2 is the total wavefront (squared) error, which is the sum of the wavefront fitting error due to a finite number of actuators and the error from the servo. For high intensities, $\sigma^2 = \sigma^2_{fit} + \sigma^2_{servo}$, where $\sigma^2_{fit} \approx 0.35(r_s/r_\circ)^{5/3}$ and $\sigma^2_{servo} = 0.96(t_d/t_o)^{5/3}$. Under the assumptions made by Vernon for the n=21 and $r_\circ =$ 0.2 m case, (and $t_\circ =$ 7.9 ms), we have $S \approx 0.45$, which is fairly close to the value of 0.54 from the simulations.

Figure Q.5 shows the fringe amplitudes for a low-order (n=6) AO case. In this case the fringe amplitudes for the 3- and 2-beam cases have been reduced to 0.26 and 0.22, respectively, close to the calculated Strehl ratio of 0.28. These results suggest a simple 'two stream model' of the beam combination — a completely coherent beam with an intensity equal to the Strehl ratio, and a completely incoherent beam that contributes to scattering the light and reducing the contrast of the fringes.

There are several conclusions to be drawn from these simulations:

- The Strehl ratio and visibility amplitudes are nearly equal. Thus, calculations of Strehl alone are sufficient to predict the visibility losses of an Array with an AO system. Furthermore, the simulations are slightly more optimistic than the analytical model of Appendix S.

- An AO system with a $S \geq 0.7$ should be a goal, and this requires at least $(D/r_\circ)^2$ actuators or Zernike modes of correction. (Simulations have shown that for higher order AO the deformable mirror (DM) and wave-front sensor (WFS) geometry have
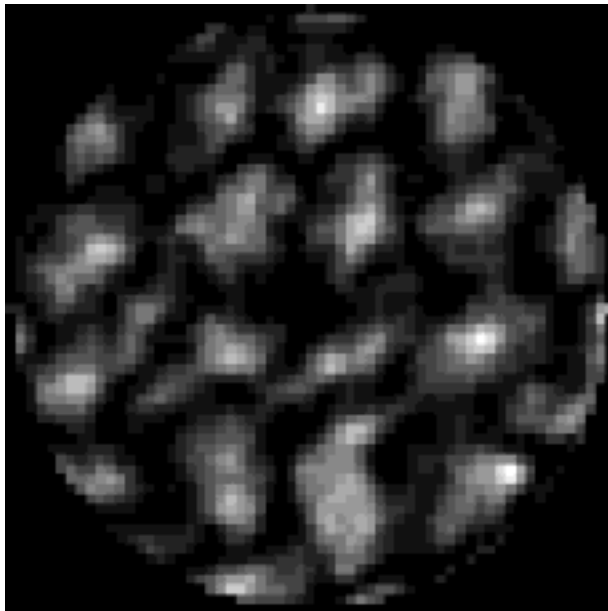
FIGURE Q.2. Simulated fringe pattern for 3-beam combination: $r_o = 20\,\mathrm{cm}$; AO with 21 Zernike modes; servo BW = 40 Hz; additional processing lag of 18 ms (3.5 steps); no photon noise.

little effect on the performance.) Because the visibilities vary greatly with r_o in an actual system, it will be more difficult to obtain high visibility accuracies in operating with low visibilities, because of variations in r_o between target and calibration source.

- Photon noise reduces the visibility significantly for simulations with 30 photons per actuator element. Thus, the analytical estimate of 50 photons in both Appendices O and S as a practical limit appears reasonable.

Q.3.2. Magnitude Limit Estimates for Visual

A spread sheet calculator model has been developed (see Appendix R) to calculate optical throughputs and magnitude limits. Some basic results and assumptions from the throughput model are:

- **AO System** — The AO system has a bandwidth of 300 nm and a QE of 80% (a good CCD); readout noise ignored; 50 photons required per subaperture, and 50% of the light after the telescope is used for this system (or $\sim 40\%$ of the incident light).

- **Tip/Tilt System** — A CCD with 80% QE is used over a 300 nm band, 50 photons are required for tip/tilt, and $\sim 5\%$ of the incident light in the system goes for tip/tilt detection.

- **Fringe-Tracking System** — The detector bandwidth is 200 nm; 80% QE. We require 100 photons for FT.
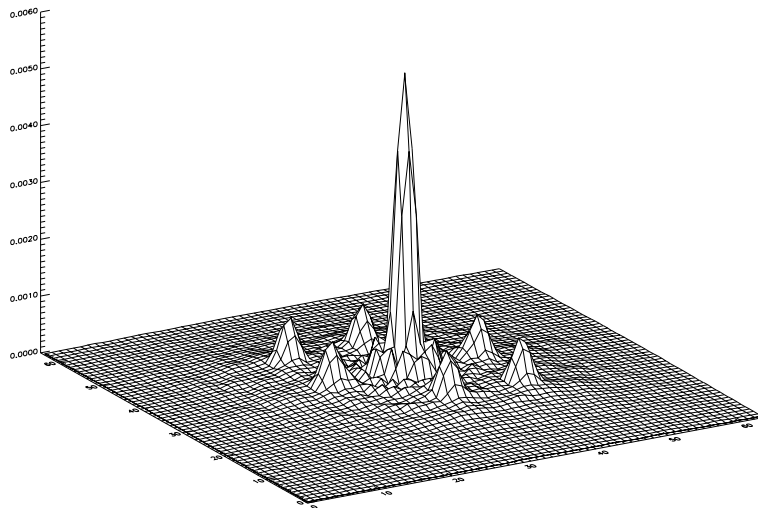
FIGURE Q.3.   Fourier amplitudes for 3-beam combination: 200 simulated frames; $r_o = 20$ cm; n=21 AO; other parameters as in Figure Q.2. Amplitudes are reduced to 0.55 of nominal. Closure phase errors are 0.25 radian.
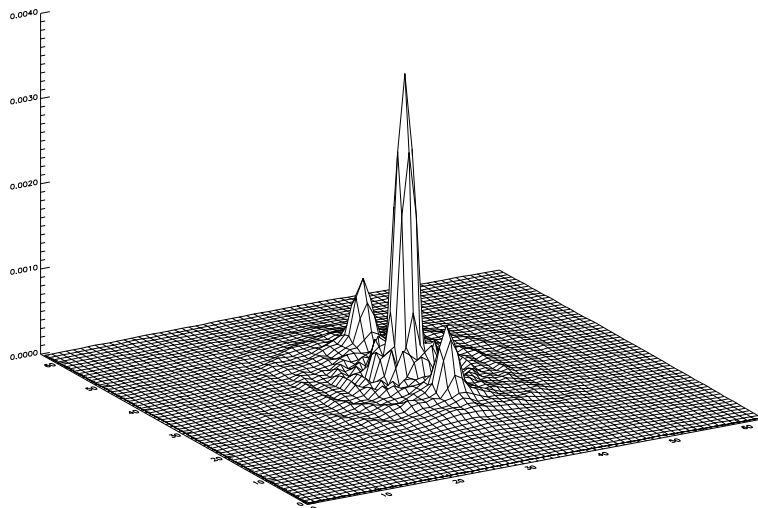

FIGURE Q.4.   Parameter amplitudes for 2-beam combination: conditions as in Figure Q.3. Amplitudes reduced to 0.54 of nominal. (No closure phase exists.)
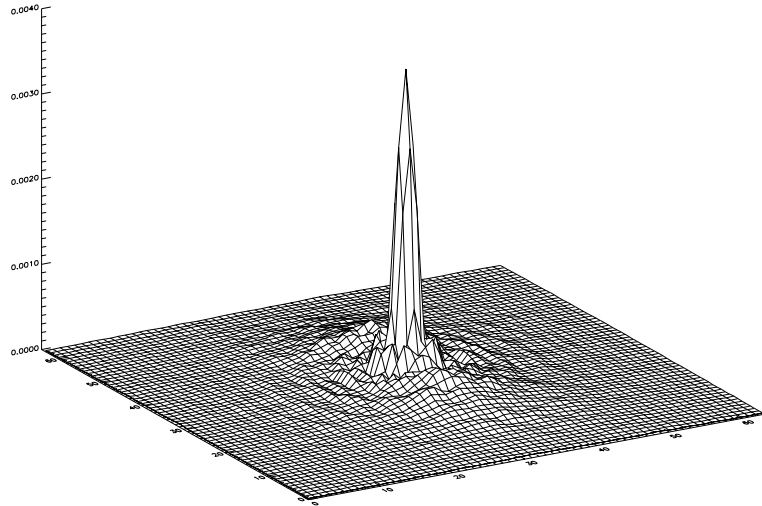
FIGURE Q.5. Fourier amplitudes for 2-beam combination: 100 simulated frames; AO with 6 Zernike modes; servo BW = 40 Hz; additional processing lag of 3.5 time steps (18 ms); no photon noise. Amplitudes are reduced to 0.22 of nominal.

- **Tracking Methodology** — The following magnitude limits are for active fringe tracking (FT). It should be possible to extend the magnitude limit by employing passive open-loop fringe tracking out to the point at which either the AO or tip/tilt system fails, which would gain as much as two magnitudes in some cases. It is for this reason that the magnitude limit in Figure Q.1 was set at 14.

- **Imaging System** — Current design calls for a DQE of only 10% for this system, which could improve if very low noise CCDs become available. Note that if this magnitude is less than that of the rest of the system, the visibilities can still be measured.

- **IR Imaging** — We do not currently plan separate tip/tilt and FT systems in the K-band IR; thus, the visual bands are still used for these purposes. For the IR cases, we have assumed apertures of 80 cm and 100 cm for average and excellent seeing cases.

In Table Q.3 we have also assumed that with a laser guide star the magnitude limit on the AO system is essentially removed. We have further assumed that using a sub-aperture of 1.5 r_o without AO is "good enough" in terms of acceptable visibility losses ($V \approx 0.8$). We also assumed a t_o of 5 and 11 ms for the $r_o = 10$ and 20 cm cases respectively. (based on $t_o \propto r_o^{1.2}$.)

Finally, we note that the available technologies seem to define three regions in which no AO, AO, and AO with laser guide stars are advantageous. Basically, small telescopes (≈ 0.3 m in V, 1.0 m in K) do not need any compensation beyond tip/tilt. Medium sized telescopes (roughly $0.7 - 1.2$ m in V and $3.3 - 5.5$ m in K) show a significant improvement with an AO system, but do not gain as much as an additional magnitude with the laser guide star. Large telescopes (>1.2 m in V and >5.5 m in K) must have a laser guide star in order to realize an aperture advantage in magnitude limit.

TABLE Q.3.   Magnitude limits for the three servos and detector.

Seeing	AO Used	Tip/Tilt	Fringe Track	High Order AO	Mag. Limit V	Mag. Limit K
Average (10 cm)	No AO	13.3	7.7	N/A	7.7	13.8
	AO	12.5	11.0	9.4	9.4	13.5
	Laser	13.3	11.8	17.0	11.8	14.3
Excellent (20 cm)	No AO	14.2	10.1	N/A	10.1	15.1
	AO	13.3	11.9	11.8	11.8	14.2
	Laser	14.1	12.7	17.0	12.7	15.1

We therefore conclude that:

- Seeing is very important, especially without AO systems. The limiting magnitude without AO improves by 2.4 and 1.3 magnitudes in V and K, respectively, between the "average" and "excellent" seeing cases.

- Introducing an AO system improves the limiting magnitude in the visual for the system by 1.7 magnitudes for both seeing cases. This improvement is due to the fact the whole telescope aperture can be used, greatly increasing the number of photons reaching the fringe-tracker, which is generally the "weak link". There is no justification for using an AO system in the IR, however.

- Using a laser guide star improves the limiting magnitude in V by an additional 2.4 and 0.9 magnitudes for the two seeing cases. In the average seeing case a laser guide star would seem advantageous but it is unclear whether this improvement justifies the extra expense. In K the laser guide star under excellent seeing just returns the system to the level of the no-AO case!

- The proposed CHARA Array 1 m telescopes are about the largest apertures that can be used without AO in K. At the same time the CHARA Array offers a gain of $2 - 3$ magnitudes over a small telescope system (≈ 30 cm) in V and K.

- Large apertures will require laser guide stars.

Q.4.   SIZE AND COMPLEXITY LIMIT

Another limitation on the performance of an interferometric array is due to the finite coverage of object visibilities in the $u - v$ plane. By the Van Cittert–Zernike Theorem the object intensity $O(x, y)$ is a Fourier transform pair with complex visibility $V(u, v)$. Along any baseline connecting two telescopes we obtain the complex visibility of the object at a single point, say (u', v'). Suppose we directly Fourier transform the observed visibility data $V'(u, v)$ in order to obtain an estimate of the object, $O'(x, y)$. Because of inadequate sampling (due to a finite number of telescopes), various spatial frequencies of the object are not measured, resulting in "sidelobes" and other objectionable features in the recovered images if the original object has significant power in the missing spatial frequencies. There are a number of techniques for trying to improve the image quality from the "dirty

image", O'. The CLEAN algorithm (Hogbom 1974, Schwarz 1978, Cornwell 1983) is an iterative technique that uses the "dirty beam" (the point spread function from the $u - v$ coverage with a point source) to produce a "cleaned image". Another faster, but somewhat lower quality, approach is to interpolate between observed visibility data points to fill in the $u - v$ plane. Both methods improve the image quality, but they can only do so much when effective $u - v$ coverage is lacking.

By "effective" coverage, we mean baselines in which the modulus of the visibility is at least 0.05. This is probably conservative in that it is possible that a fringe-tracking system could work with visibilities lower than this for bright over-resolved objects. Moreover, a fringe-tracking system will use the shortest baselines possible. Binaries with unresolved components can in principle be observed by baselines of indefinite length, but resolved stellar photospheres can only be observed by baselines below a cutoff. Stars are over-resolved when their first visibility null doesn't even reach the smallest baseline of the array. Stars are also under-resolved when the first null falls outside the largest available baseline. For each of the CHARA configurations, there is a range of stellar diameters of roughly 15:1 for which useful data can be obtained.

Q.4.1. $U - V$ Coverage and Object Image Recovery

A variety of simulations were done to estimate the quality of images that could be obtained with the CHARA Array. In these simulations, we start with the $u - v$ coverage for the A or B baseline configurations and a given observation time. We then obtain the dirty beam and dirty image for a given object and attempt to reconstruct the image with CLEAN and visibility interpolation techniques. We have used Cornwell's (1983) modification of CLEAN to improve the smoothness of the images. The visibility interpolation is done by triangular linear interpolation between the 'observed' visibility points. The resulting reconstructed images show approximately what can be done with a given array configuration and number of observations. (In some simulations we have also included the effects of partially filling in the $u - v$ plane by observing over a wide wavelength range.)

Figure Q.6 shows an 18-star "cluster" imaged by the array. Note the complex fringe pattern in the $u-v$ coverage (upper right). In general, images such as a star cluster with unresolved point sources are easier to recover, because the fringe patterns extend over all the $u - v$ coverage of the array. In resolved systems, as in Figure Q.7, only a subset of baselines are effective. In this figure, we see reconstructed images of a binary with two resolved photospheres, tidal and radiative distortions, and limb-darkening. Note that the dirty image doesn't even show a distinct secondary star, but that both stars are clearly visible after CLEAN and visibility interpolation. Figure Q.8 shows what happens when stellar disks are over-resolved: eventually only the shortest baselines provide any information about the object. Finally, Figure Q.9 shows the results of fast "snapshot" $u - v$ coverage *versus* repeat observations to expand the $u - v$ coverage. Note that even the "snapshot" mode provides reasonable images of simple objects. A further improvement which we have simulated occurs for observations with a large enough spectral range, i.e. $\Delta\lambda/\lambda \approx 0.2$.

Q.4.2. Object Resolution and Magnitude Limits

In Figure Q.8 it is obvious that stars can be over-resolved as well as under-resolved. Figure Q.10 shows the region of stellar photospheres accessible to the CHARA Array "A" configuration, which has a maximum baseline of 354 m. A given stellar temperature defines a surface brightness at 600 nm, which gives an upper and lower limit on stellar magnitudes
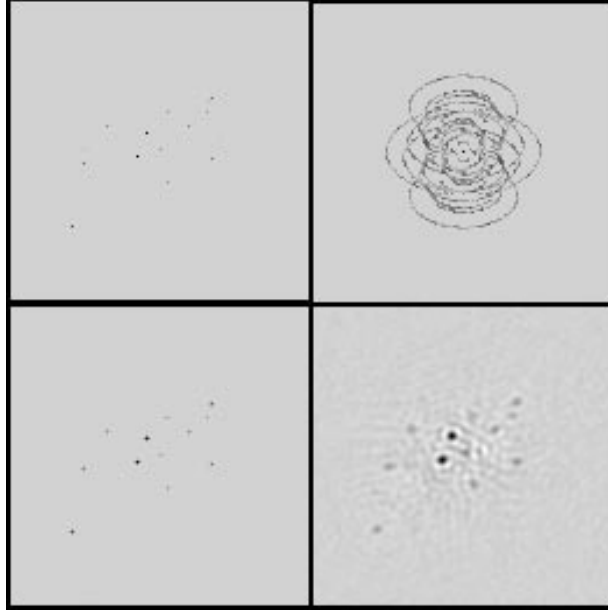
FIGURE Q.6. A resolved cluster. Top Left: star cluster, the object. Top Right: modulus of visibilities. The two images in the bottom row are the resulting cleaned image on the left and the interpolated image on the right.

for the upper and lower limits on sizes the array can resolve. For the CHARA "B" configuration, these limits move upward about 2.3 magnitudes. It is evident that stars of every spectral class can be resolved with the CHARA Array (This is one reason why this set of baselines was chosen.) This figure is pessimistic in the sense that if any significant small bright or dark surface features exist on the photospheres, they can be imaged, even if the star is in the "over-resolved" region.

Q.5. CONCLUSIONS

The test of any scientific instrument's performance is ultimately what science can be done with it. The four performance dimensions of the CHARA Array were: 1) the maximum resolution, 2) the magnitude limit, 3) the size and complexity of the objects that can be imaged with it, and 4) the operating wavebands.

In terms of criterion 4) above, the Array is designed to operate primarily in two wavebands, both 0.55–0.9 μm ($\approx V$, R, and I), and 2.1–2.5 μm ($\approx K$).

High resolution of visual objects, criterion 1), requires a long maximum baseline. The maximum resolution of the longest baseline (354 m) at 550 nm is 0.16 and 0.39 milliarcseconds for binaries and resolved stars, respectively.

Somewhat lower resolution of more complex K-band objects (e.g. YSO's) dictated good $u - v$ plane coverage over smaller baselines. The CHARA design, with seven telescopes that can be positioned into two configurations, attempts to adress these needs. We have shown that complex objects could be imaged with the CHARA Array (performance criterion 3).

Finally, our choice of 1 m apertures was again a design compromise. The CHARA Array
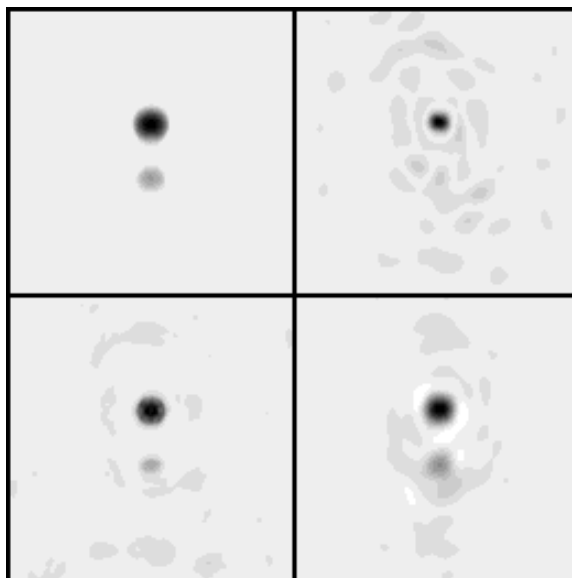
FIGURE Q.7.   An example of the image quality improvement using the CLEAN or interpolation methods. The top left box is the object, a binary system with both stars resolved including limb darkening. The top right box is the dirty image obtained using the A configuration. The two images in the bottom row are the resulting cleaned image on the left and the interpolated image on the right. The cleaned image is superior but took much longer to calculate.
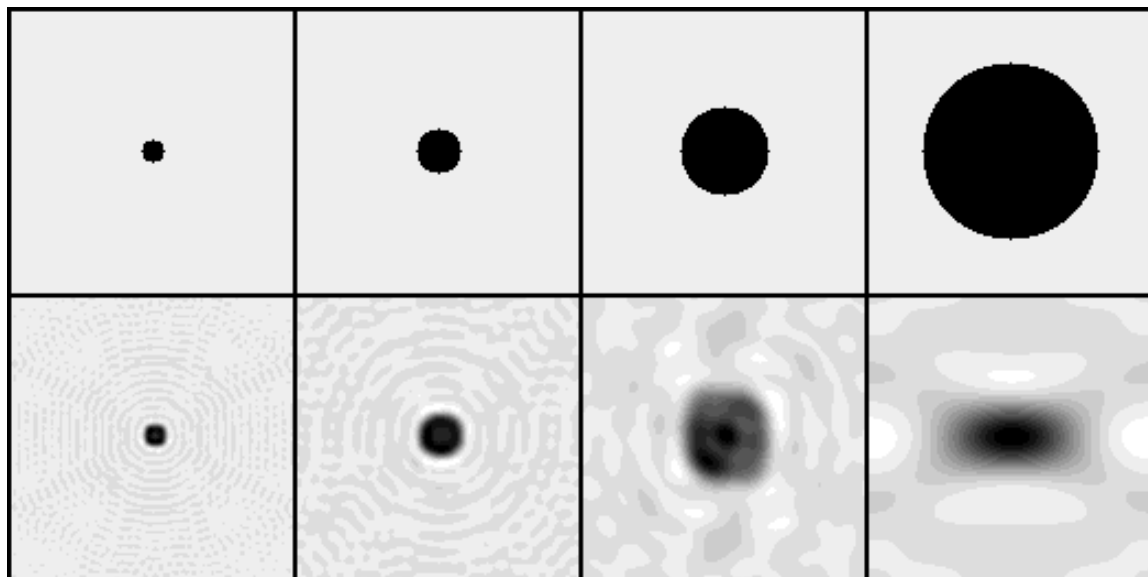

FIGURE Q.8.   Stars of various sizes (top) along with their images using the interpolative method. The stellar diameters are, from left to right, 5, 10, 20 and 40 pixels where a pixel is $306.4 \times \lambda$ arcseconds. For example at 0.5 microns the images would be 0.77, 1.53, 3.06 and 6.12 milliarcseconds. The effect of over-resolution is clear in the largest objects. For these objects the B configuration would need to be used.
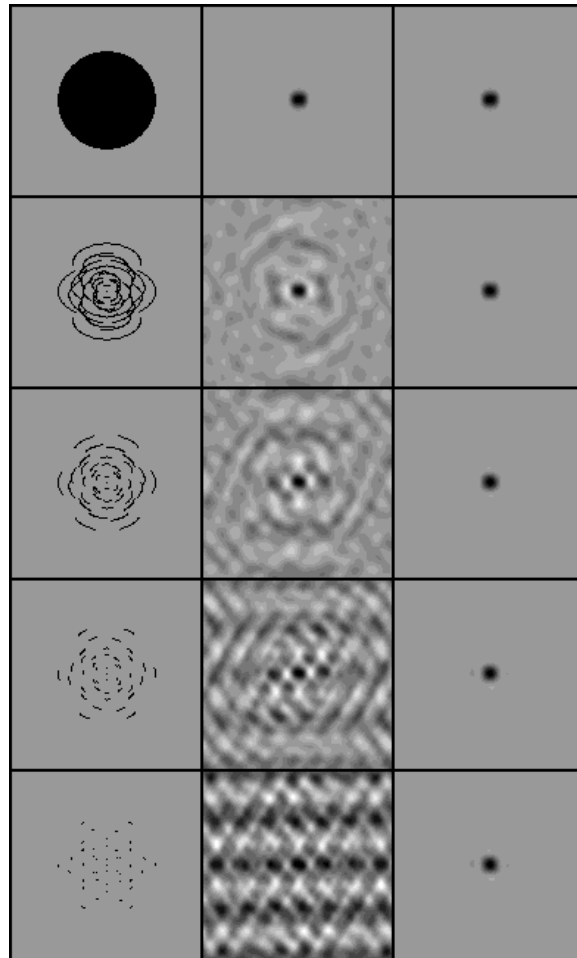
FIGURE Q.9.   An illustration of imaging a resolved star with limb darkening using different $u - v$ plane coverages. In each row the box on the left shows the $u - v$ plane coverage, with a full aperture on the top and a 'snapshot' coverage on the bottom. The picture in the middle is the resulting dirty image and an interpolated image is shown on the right. While the dirty image degrades quickly, the interpolated image maintains good quality. For simple objects, a snapshot mode supplies sufficient $u - v$ plane coverage for the array to supply good images.
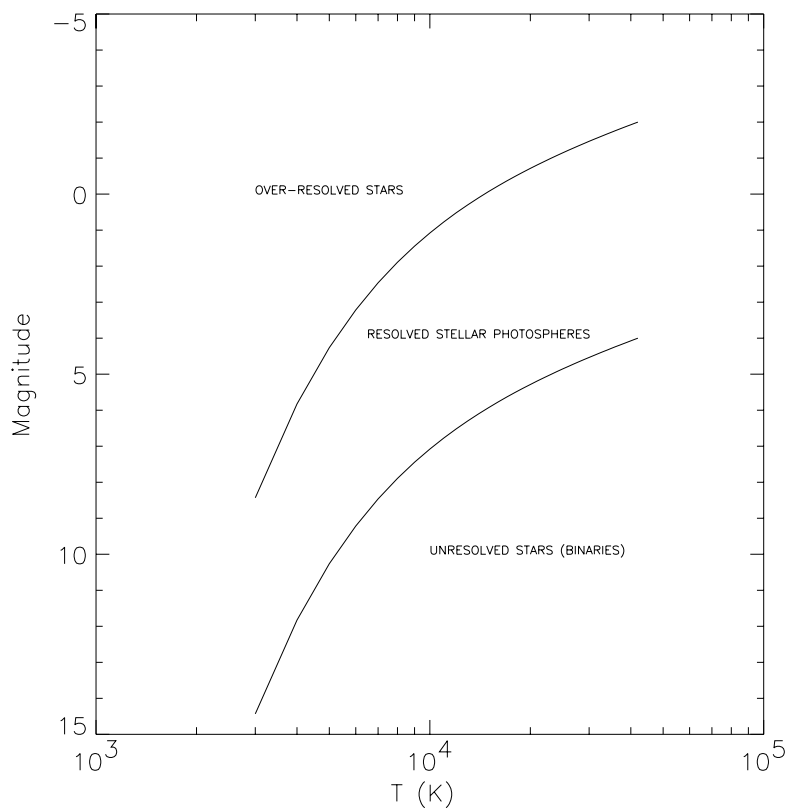
FIGURE Q.10. The projected performance of the Array for various stellar magnitudes and classifications. In the top left section of the plot, stellar atmospheres are over-resolved, and the contracted B configuration of the Array would be required. Alternatively the objects in this section could be studied using aperture masking or speckle techniques. On the bottom right, stellar atmospheres will be unresolved but multiple star systems, such as binaries, could be studied. Between these two sections a regime of resolved stellar photospheres occurs.

can go as deeply as 15th magnitude in K and 10th in V under good conditions without an AO system (criterion 2). With an AO system plus laser guide star a visual magnitude of nearly 13 could be attained. These magnitude limits should allow, for example, the imaging of even M dwarfs (in V) or AGN's (in K).

Q.6.   REFERENCES

Cole, W.A., Fekel, F.C., Hartkopf, W.I., McAlister, H.A., & Tomkin, J., 1992, *AJ*, **103**, 1357
Cornwell, T.J., 1983 *A&A*, **121**, 281
Hogbom, J.A., 1974 *A&AS*, **15**, 417
Schwarz, U.J., 1978, *A&A*, **65**, 345